SUSTAINABLE FILMS FROM WATER HYACINTH CELLULOSE: MECHANICAL AND THERMAL CHARACTERIZATION OF PLASTICIZED CMC

USARAT RATAKAMNUAN,[*] NITTAYA KLANGPINIT[*] and PRACHAYA NAMWONG[**]

[*]*Industry Chemistry Innovation Programme, Faculty of Science, Maejo University, Chiang Mai, 50290, Thailand*
[**]*Division of Science, Faculty of Science and Agricultural Technology, Rajamangala University of Technology Lanna, Chiang Mai, 50300, Thailand*
✉ *Corresponding author: U. Ratanakamnuan, usarat@mju.ac.th*

Received January 6, 2026

Water hyacinth (*Eichhornia crassipes*) was utilized as an alternative lignocellulosic source for the preparation of carboxymethyl cellulose (CMC) and the fabrication of cellulose-based films. Microcrystalline cellulose (MCC) was isolated through alkaline delignification, bleaching, and acid hydrolysis, followed by carboxymethylation using monochloroacetic acid. The successful conversion of MCC to CMC was confirmed by Fourier Transform Infrared (FTIR) and X-ray diffraction (XRD) analyses, indicating the introduction of carboxymethyl functional groups and a transition from a semicrystalline cellulose I structure to a predominantly amorphous CMC phase. Solvent-cast CMC films exhibited good transparency and homogeneity but limited ductility. To modify the mechanical performance, glycerol (G), propylene glycol (PPG), and sorbitol (S) were incorporated as plasticizers at concentrations ranging from 0 to 20% (w/w). The addition of plasticizers significantly increased elongation at break, accompanied by reductions in tensile strength and Young's modulus, reflecting enhanced chain mobility. Thermogravimetric analysis (TGA) revealed a moderate decrease in thermal stability with plasticizer incorporation. The results demonstrate that the mechanical and thermal properties of water-hyacinth-derived CMC films can be effectively tailored through plasticizer type and concentration, highlighting their potential as tunable cellulose-based film materials.

Keywords: carboxymethylcellulose (CMC), *Eichhornia crassipes*, etherification, glycerol, propylene glycol, sorbitol

INTRODUCTION

Cellulose-based polymers have attracted sustained interest due to their structural versatility, easy chemical modification, and suitability for conversion into functional materials. Among cellulose derivatives, carboxymethyl cellulose (CMC) is one of the most widely utilized owing to its water solubility, film-forming ability, and tunable physicochemical properties. CMC has been extensively applied in areas such as coatings, binders, membranes, and functional films, where control over mechanical performance and thermal behavior is critical. The properties of CMC are strongly governed by its degree of substitution, molecular conformation, and intermolecular interactions within the polymer matrix.

Traditionally, CMC is derived from conventional cellulose sources, such as wood pulp and cotton linters. However, the high demand for cellulose-based products calls for alternative and more sustainable raw materials. In this context, agricultural residues and invasive plant species have been explored as viable feedstocks for cellulose extraction. Water hyacinth (*Eichhornia crassipes*), an aggressive aquatic weed, stands out as a particularly attractive candidate. Known for its rapid growth and ability to form dense mats on water surfaces, water hyacinth has caused widespread ecological and socio-economic problems in tropical and subtropical regions. Its proliferation disrupts aquatic ecosystems by blocking sunlight, reducing dissolved oxygen, and altering water chemistry, while also impeding navigation, irrigation, and fisheries.[1-2]

In countries like Thailand, where water hyacinth infestations are extensive, various efforts have been directed towards converting this

invasive biomass into useful products. Notably, water hyacinth has been identified as a rich source of cellulose, containing approximately 25-27% cellulose, along with 20-30% hemicelluloses and 3-10% lignin.[2-3]

Some reports have cited even higher cellulose contents, reaching up to 60%, depending on sources, tissues, growth state of water hyacinth, and extraction methods.[4] Water hyacinth has been extensively studied for its potential as a lignocellulosic biomass resource due to its high cellulose and hemicellulose contents. Several researchers have reported the successful extraction of cellulose from water hyacinth, indicating its suitability as a raw material for value-added bioproducts.[1] Previous studies have demonstrated the potential of water hyacinth in the production of microcrystalline cellulose (MCC) from water hyacinth,[5-8] while subsequent studies have explored its application in polymer reinforced composite. More recently, attention has shifted towards the synthesis of CMC from water hyacinth cellulose as a route to produce biodegradable bioplastics, offering dual environmental benefits: controlling invasive plant populations and reducing reliance on petroleum-based plastics. However, despite its promise, CMC-based bioplastic films often exhibit mechanical limitations, particularly brittleness, which hinders their wider adoption in packaging and related applications. Plasticizers, such as glycerol (G), propylene glycol (PPG), and sorbitol (S), have been commonly employed to improve the flexibility and tensile properties of CMC films.[9-12] The plasticization mechanism involves disrupting intermolecular hydrogen bonding within the polymer matrix, thereby enhancing chain mobility and flexibility.[13-15] The plasticizer significantly influences not only mechanical properties, but also thermal stability, water vapor permeability, and biodegradation rate of CMC films.[16-17]

In this study, water hyacinth-derived MCC was chemically modified into CMC and processed into solvent-cast films. The effects of G, PPG, and S at varying concentrations (0–20% w/w) on the structural, mechanical, and thermal properties of CMC films were systematically investigated. The findings provide an insight into the role of plasticizer–cellulose interactions in tailoring the performance of cellulose-based films derived from alternative lignocellulosic biomass.

EXPERIMENTAL

Materials

Water hyacinth (*Eichhornia crassipes*) was collected from natural freshwater sources in Chiang Mai Province, Thailand. Sodium hydroxide (NaOH) and sulfuric acid (H_2SO_4) were obtained from RCL Labscan Limited (Thailand). Hydrogen peroxide (H_2O_2) was supplied by QRëC™, while absolute ethanol (EtOH) was purchased from J.T. Baker. Methanol (MeOH), glycerol, and propylene glycol were sourced from Ajax Finechem. Monochloroacetic acid (MCA) and sorbitol were purchased from Loba Chemie. Glycerol, propylene glycol, and sorbitol were used as plasticizers in the preparation of CMC films. Isopropanol (IPA) was provided by QREC (ASIA) SDN BHD. All reagents were of analytical grade and used as received without additional purification.

Isolation of MCC from water hyacinth

MCC was isolated from water hyacinth biomass through a multistep chemical treatment consisting of alkaline delignification, oxidative bleaching, and acid hydrolysis. The harvested plants were thoroughly washed, cut into small pieces, and oven-dried at 60 °C for 2 h under vacuum conditions. Dried biomass (50 g) was treated with 0.5 M sodium hydroxide at 80 °C for 4 h to remove non-cellulosic components. The resulting pulp was subsequently bleached using a hydrogen peroxide solution (5% v/v) in 0.5 M sodium hydroxide at 60 °C for 4 h.

After bleaching, the cellulose-rich residue was washed with distilled water until neutral pH was attained and then subjected to acid hydrolysis using 55% (v/v) sulfuric acid at 35 °C for 30 min. The hydrolysis reaction was terminated by dilution with distilled water, followed by filtration and repeated washing to remove residual acid. The obtained MCC was dried, mechanically ground, and passed through a 250 µm sieve prior to further use. The extraction procedure was adapted from previously reported methods with minor modifications.[12] The MCC yield after each treatment step was determined according to Equation (1):

$$\% \text{ MCC content} = \frac{\text{weight of MCC (g)}}{\text{weight of dry water hyacinth (g)}} \times 100 \qquad (1)$$

Synthesis of CMC

CMC was synthesized following the procedure described by Rachtanapun *et al*.[18] with slight modifications. Fifteen grams of water hyacinth MCC powder were mixed with 50 mL of 30% (w/v) sodium hydroxide solution and 450 mL of isopropanol, stirred at room temperature for 30 minutes. Eighteen grams of monochloroacetic acid were added, and the reaction mixture was stirred for 1.5 hours, then maintained at 55 °C for 3 hours. Upon completion, the mixture separated into two phases.

The solid phase was suspended in 70 mL/100 mL methanol (100 mL) and neutralized with glacial acetic acid after the liquid phase was disposed of. After filtering and washing five times with 70 mL/100 mL ethanol (300 mL), the solid phase suspended in methanol was removed. After that, it was cleaned with pure methanol and filtered once more. The resultant CMC was produced by drying the filtration residue overnight at 55 °C in a hot air oven. After synthesis, the CMC product was in powder form. Equation (2) was used to calculate the percentage yield of CMC following synthesis:

$$\%\text{CMC content} = \frac{\text{weight of CMC (g)}}{\text{weight of water hyacinth MCC (g)}} \text{x}100 \quad (2)$$

Fourier Transform Infrared (FTIR) Spectroscopy

The functional groups and chemical structures of water hyacinth-derived MCC and CMC were analyzed using FTIR Spectroscopy (Spectrum RX1, PerkinElmer, Inc., US). Samples were prepared by mixing 1 part sample with 10 parts potassium bromide (KBr), ground thoroughly in an agate mortar until homogeneous, and pressed into thin pellets using a hydraulic press at 1500-2000 psi for 1-2 minutes. The spectra were recorded in the wavenumber range of 4000–600 cm^{-1}.

X-ray Diffraction (XRD) Analysis

The crystalline structure of MCC and CMC samples were examined by XRD using an Empyrean Series 3 Diffractometer (Malvern Panalytical, Netherlands). Measurements were performed using Cu Kα radiation, and diffraction patterns were collected over a 2θ range of 10-90° to identify crystalline phases and assess structural changes resulting from chemical modification.

Preparation of CMC films

Film-forming solutions were prepared by dissolving and stirring 1.8 g of CMC powder in 60 mL of distilled water at 40 °C for 15 hours. After cooling to room temperature, varying amounts (0-20% w/w based on CMC content) of plasticizers (G, PPG, or S) were added, and the mixture was stirred until homogeneous. The solution was cast onto 15 cm diameter Petri dishes and dried overnight in a hot air oven at 40 °C. Dried films were stored under dry conditions prior to testing. Film thickness was measured using a micrometer.

Thermal properties

Thermal stability and decomposition profiles of water hyacinth-derived CMC films were determined by thermogravimetric analysis (TGA) using a Thermoplus TG8120 instrument (Rigaku Corporation, Japan). Samples were first dried at 60 °C for 24 hours prior to testing. Thermal analysis was performed under a nitrogen atmosphere, heating from 30 °C to 600 °C at a rate of 10 °C/min. Films prepared with varying plasticizer types (G, PPG, and S) and concentrations were analyzed to assess the effect of plasticizers on thermal behavior.

Tensile properties

The mechanical properties of the CMC films, including tensile strength, Young's modulus, and elongation at break, were evaluated using a Universal Testing Machine (Zwick/Roell, Germany) following ASTM D882 standard. Film specimens with a width of 1.00 cm and gauge length of 5.00 cm were tested at a crosshead speed of 125 mm/min. Each film sample was tested in five replicates, and average values were reported.

RESULTS AND DISCUSSION

% MCC content

MCC is derived from the alpha-cellulose fraction of lignocellulosic biomass through controlled hydrolysis, typically using acid treatment. Equation (1) was used to determine the MCC content following the delignification, bleaching, and hydrolysis processes. The MCC content of water hyacinth is 17.82 ± 1.27%

%CMC content

MCC from water hyacinth was extracted and then synthesized to CMC with monochloroacetic acid in the presence of an aqueous alkali. After synthesis, the percentage yield of CMC was determined using Equation (2). The percentage content of CMC extracted from water hyacinth cellulose was 160.67%. According to Kamthai S. and Magaraphan R.,[19] %CMC obtained from the bleached bagasse pulp was 81.83% at the same aqueous sodium hydroxide concentration (30%, w/v) for alkalization reaction. However, this data was consistent with earlier findings, which showed that a similar NaOH concentration (30% (w/v)) produced roughly 165% of durian rind CMC.[18]

Cellulose is activated using aqueous NaOH in an organic solvent slurry, which then combines with the cellulose and monochloroacetic acid as an etherifying agent to produce CMC. This behavior can be explained by the carboxymethylation process, as described by Barai *et al*.[20] The hydroxyl groups of the cellulose chains are stimulated and changed into a more reactive alkaline form during the alkalization phase, which is the initial stage of the carboxymethylation process.

$$\text{Cellulose-OH} + \text{NaOH} \longrightarrow \text{Cellulose-ONa} + H_2O \quad (3)$$

Subsequently, etherification occurs as in Equation (4) to produce CMC, and a side reaction

occurs as in Equation (5) to produce sodium glycolate:

$$\text{Cellulose-ONa} + \text{ClCH}_2\text{COOH} \longrightarrow \text{Cellulose-OCH}_2\text{COONa} + \text{NaCl} \quad (4)$$

$$\text{ClCH}_2\text{COONa} + \text{NaOH} \longrightarrow \text{CH}_2\text{COONa} + \text{NaCl} \quad (5)$$

FTIR spectroscopy

The chemical structure and functional groups of MCC and CMC derived from water hyacinth were characterized using FTIR spectroscopy. The infrared absorption bands are summarized in Table 1, and the corresponding FTIR spectra are presented in Figure 1. The FTIR spectrum of water hyacinth-derived MCC exhibited prominent peaks at 3336 cm^{-1}, corresponding to O-H stretching vibrations, indicating the presence of hydroxyl groups. The absorption band at 2885 cm^{-1} was assigned to C-H stretching vibrations of the hydrocarbon groups.

A peak observed at 1640 cm^{-1} was attributed to absorbed water molecules within the cellulose structure. Additionally, characteristic peaks at 1429 cm^{-1} (CH_2 bending), 1368 cm^{-1} (C-H bending) and 1030 cm^{-1} (C-O-C stretching), and 896 cm^{-1} (β-glycosidic linkages) confirmed the cellulose backbone structure.

In contrast, the FTIR spectrum of the synthesized CMC displayed distinct differences compared to MCC revealing chemical modifications. The broad peak at 3266 cm^{-1}, representing O-H stretching, and the band at 2936 and 2882 cm^{-1} for C-H stretching appeared with reduced intensity, suggesting successful chemical modification. Notably, a new prominent peak at 1586 cm^{-1} was observed, corresponding to the C=O stretching vibration of carboxylate groups, indicating the introduction of carboxymethyl substituents.

The peak at 1045 cm^{-1}, assigned to C-O stretching, while the absorbed peak at 1412 cm^{-1} is attributed to the salts of carboxyl groups (COONa) further confirmed the presence of ether linkages characteristic of carboxymethylation. These spectral changes validate the successful substitution of hydroxyl groups in the cellulose backbone with carboxymethyl groups during the synthesis process.

XRD analysis

The crystalline structure of MCC derived from water hyacinth and its carboxymethylated derivative was investigated using XRD. The diffraction patterns are presented in Figure 2. The XRD pattern of MCC exhibited characteristic diffraction peaks at 2θ values of approximately 15.38°, 22.29°, and 35°, which correspond to the (110), (200), and (004) crystalline planes of cellulose I, respectively.[21-24] These peaks are indicative of the semicrystalline nature of cellulose, consistent with previous reports on lignocellulosic MCC. The sharp and intense peak around 22.6° confirms the high degree of crystallinity and a well-ordered structure of MCC.

Table 1
FTIR absorption bands of MCC and CMC derived from water hyacinth

Sample	Wavenumber (cm^{-1})	Band assignment
MCC	3336	O-H stretching (hydroxyl groups)
	2885	C-H stretching (aliphatic)
	1640	H-O-H bending (absorbed H_2O)
	1429	CH_2 bending / crystalline cellulose indicator
	1368	C-H bending
	1315	O–H bending
	1030	C–O–C stretching (glycosidic linkage)/ C-O stretching of ether linkage
	896	β-glycosidic linkage
CMC	3266	O-H stretching (hydroxyl groups)
	2936, 2882	C-H stretching (aliphatic)
	1586	C=O asymmetric stretching of COO^- (carboxylate group)
	1412	C-O symmetric stretching of COO^-
	1322	O–H bending
	1045	C–O–C stretching (ether linkage)

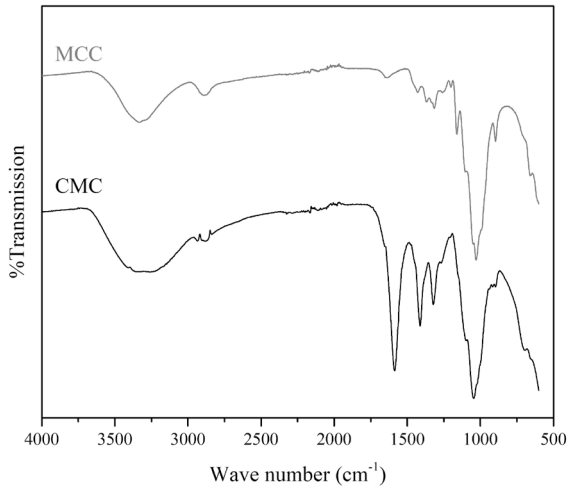

Figure 1: FTIR spectra of MCC and CMC extracted from water hyacinth

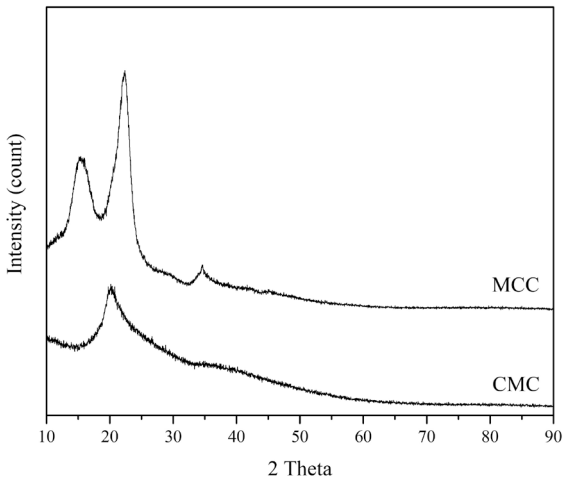

Figure 2: XRD patterns of MCC and CMC from water hyacinth

In contrast, the XRD pattern of CMC displayed a broad diffraction band centered at around 2θ=20°, with the absence of distinct crystalline peaks observed in MCC. This characteristic broad peak indicates the amorphous nature of CMC. The carboxymethylation process, which involves the substitution of hydroxyl groups on the cellulose backbone with carboxymethyl groups, disrupts the highly ordered hydrogen bonding network present in crystalline cellulose. The introduction of carboxymethyl groups and the substitution at the hydroxyl sites interfered with the hydrogen bonding network, leading to a loss of crystallinity. The reduction in crystallinity upon carboxymethylation is advantageous for various applications, as it enhances the solubility and film-forming ability of CMC. These structural modifications were confirmed by the absence of sharp peaks in the CMC pattern, indicating a transition from semicrystalline cellulose to predominantly amorphous CMC.

Effect of plasticizer on physical appearance of CMC films

Following the successful synthesis and structural confirmation of CMC derived from water hyacinth, solvent-cast CMC films were prepared. Distilled water was used as the casting solvent, and three types of plasticizers – G, PPG, and S – were incorporated at varying concentrations. G and PPG were added at 5%, 10%, 15% and 20% (w/w based on CMC content), while S was added at 2.5%, 5%, 10% and 15% (w/w) due to formulation constraints observed at higher concentrations. The films were cast in 15 cm diameter Petri dishes and dried under controlled conditions.

The physical appearance of the unplasticized CMC film is presented in Figure 3. The film exhibited a smooth surface, clear and transparent appearance, and good flexibility. These characteristics are indicative of the homogeneous dispersion and successful film formation of water hyacinth-derived CMC.

Figures 4 to 6 show the appearance of CMC films plasticized with varying levels of G, PPG, and S, respectively. All plasticized films retained a uniform and continuous structure. Films incorporating G and PPG at different concentrations displayed no significant changes in appearance; they remained smooth, transparent, and flexible, similar to the neat CMC film. However, films plasticized with S exhibited a slight increase in opacity compared to the unplasticized CMC films, indicating minor phase separation or aggregation at higher S levels.

Notably, S incorporation was limited to a maximum of 15% (w/w), as formulations with higher concentrations resulted in phase migration, with visible exudation of plasticizer on the film surface, leading to unsuccessful film formation. Therefore, S loading beyond this threshold was excluded from further testing.

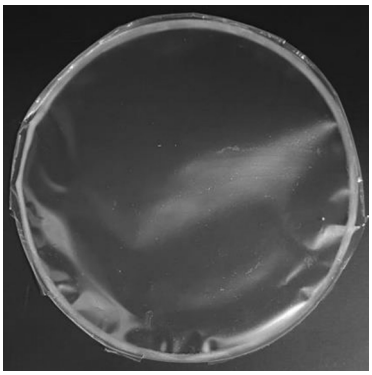

Figure 3: Physical appearance of neat CMC film derived from water hyacinth without any plasticizer addition

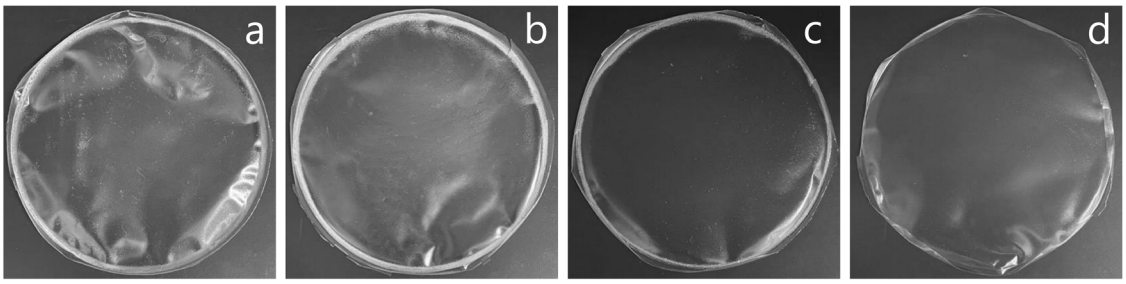

Figure 4: CMC films plasticized with glycerol at (a) 5%, (b) 10%, (c) 15%, and (d) 20% w/w concentrations

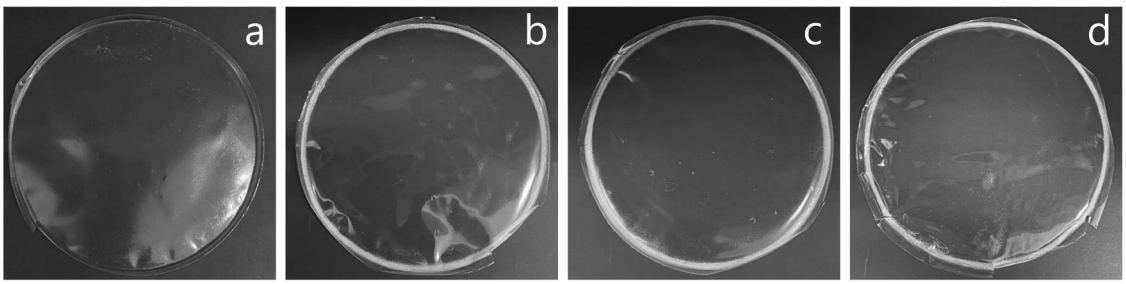

Figure 5: CMC films plasticized with propylene glycol at (a) 5%, (b) 10%, (c) 15%, and (d) 20% w/w concentrations

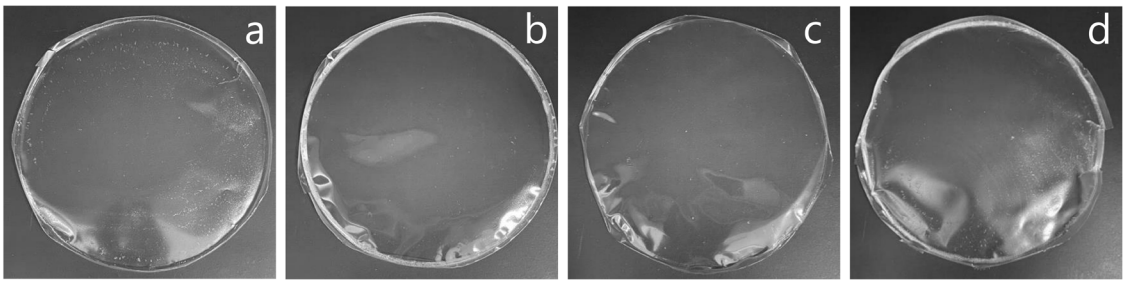

Figure 6: CMC films plasticized with sorbitol at (a) 2.5%, (b) 5%, (c) 10%, and (d) 15% w/w concentrations

Effect of plasticizer on crystallinity of CMC films by X-ray diffraction

Figure 7 presents the XRD patterns of CMC films from water hyacinth and CMC films plasticized with varying concentrations of G, PPG, and S. The XRD pattern of the unplasticized CMC film exhibits a characteristic broad halo centered around $2\theta \approx 20°$, confirming its predominantly amorphous nature, consistent with previous reports on CMC. This broad peak arises from the disordered arrangement of the polymer chains due to the carboxymethyl substitution, which disrupts the regular hydrogen bonding network of cellulose.

The continuous existence of the broad halo in all plasticized samples shows that the general amorphous nature of the CMC films is preserved upon the addition of various plasticizers. However, subtle changes in the shape and intensity of this halo can be observed, indicating the influence of the plasticizers on the molecular arrangement

within the CMC matrix. The degree of change in the XRD patterns appears to be influenced by both the type and concentration of the plasticizer. The XRD patterns of CMC films plasticized with 5% G (CMC 5G) and 20% G (CMC 20G) show a slight broadening of the amorphous halo and a subtle shift towards lower 2θ values compared to the unplasticized CMC. This suggests that G, a small molecule plasticizer, effectively penetrates the CMC matrix, increasing the interchain spacing and enhancing molecular mobility. The higher concentration of G (20%) appears to result in a more pronounced broadening, indicating a further increase in the amorphous character and a reduction in any residual ordered domains. The obtained data are in line with previously published results.[25-27]

Similarly, the incorporation of PPG at concentrations of 5% (CMC 5PPG), 15% (CMC 15PPG), and 20% (CMC 20PPG) also results in XRD patterns characteristic of amorphous materials. A broadening of the halo is observed with increasing PPG concentration, suggesting that PPG, a larger polymeric plasticizer, also disrupts the intermolecular interactions within the CMC matrix, leading to increased chain flexibility and a more disordered structure. The effect seems to be more gradual with increasing PPG concentration compared to G. The findings of this study are consistent with those reported by Basu P. *et al*.,[28] who observed a decrease in the intensity of crystalline peaks in CMC films with increasing PPG concentration, suggesting a more amorphous structure.

The XRD patterns of CMC films plasticized with 2.5% S (CMC 2.5S) and 5% S (CMC 5S) also display the broad amorphous halo. The addition of S appears to have a similar effect to G, increasing the interchain distance and enhancing the amorphous nature of the CMC film. The broadening of the halo is more evident at the higher S concentration (5%). The present results support the conclusions drawn in the work of Tamara T. *et al*.[29] that discusses the role of S in increasing molecular mobility, which is often associated with a more amorphous structure.

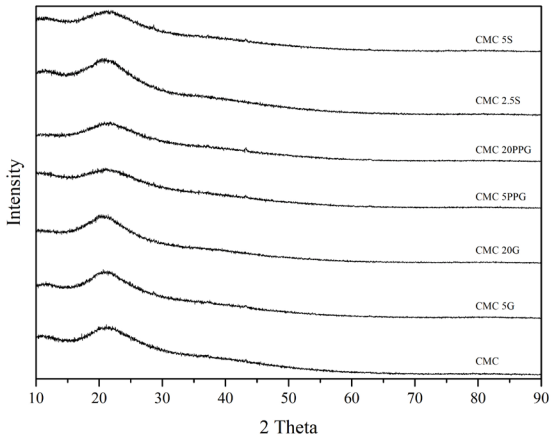

Figure 7: XRD patterns of unplasticized CMC film (CMC) and CMC films plasticized with different concentrations of glycerol, propylene glycol, and sorbitol.

Effect of plasticizer on tensile properties of CMC films

The tensile properties of CMC films derived from water hyacinth were evaluated according to ASTM D882. Film specimens were cut into strips with a width of 1.00 cm, and their thickness was measured to calculate the cross-sectional area. The tests were conducted using a universal testing machine with a gauge length of 5.00 cm and a crosshead speed of 5 mm/min until film breakage occurred. Based on the cross-sectional area (A), the maximum tensile force (F), and the elongation at break (ΔL), the tensile strength (σ), elongation at break (%), and Young's modulus (E) were calculated for CMC films without plasticizer and those containing different types and concentrations of plasticizers.

As shown in Figure 8, the unplasticized CMC film exhibited a tensile strength of 34.14 MPa. Upon the addition of G, the tensile strength gradually decreased with increasing plasticizer concentration. For PPG, the overall tensile strength was lower than that of the unplasticized film. Interestingly, increasing the concentration of PPG from 5% to 15% (w/w) slightly improved tensile strength, but a further increase to 20% (w/w) led to

a decline. Overall, CMC films plasticized with PPG remained weaker than the control. In the case of S, a tensile strength of 35.79 MPa was recorded at the lowest tested concentration of 2.5% (w/w), which was comparable to the unplasticized film. However, increasing the S concentration from 5% to 15% (w/w) resulted in a steady reduction in tensile strength. Notably, at 20% (w/w), S led to phase separation and plasticizer blooming, making film formation unsuccessful.

As illustrated in Figure 9, the elongation at break of the unplasticized film was 9.52%. Upon the incorporation of plasticizers (G, PPG, and S), elongation at break increased with higher plasticizer content. Among the plasticizers, G had the most significant effect, yielding the highest elongation of 87.96% at 20% (w/w). This trend aligns with the lubricity theory, which explains how plasticizers reduce intermolecular friction and facilitate polymer chain mobility.

Figure 10 shows the variation in Young's modulus of the films. The unplasticized CMC film had the highest modulus at 431.27 MPa. The addition of plasticizers led to a marked reduction in stiffness, with Young's modulus decreasing as the plasticizer concentration increased. This is consistent with the expected effect of plasticizers, which reduce film rigidity by increasing molecular mobility.

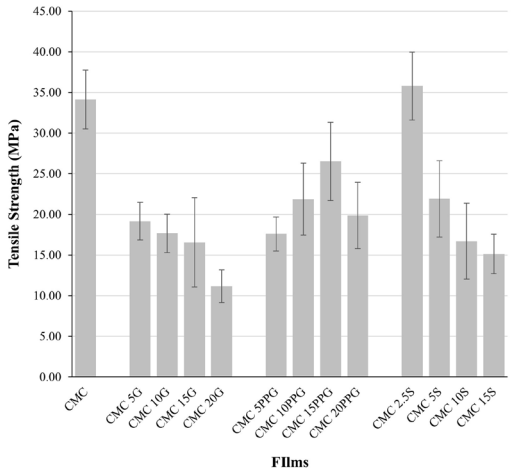

Figure 8: Tensile strength of CMC films with different concentrations of glycerol, propylene glycol, and sorbitol

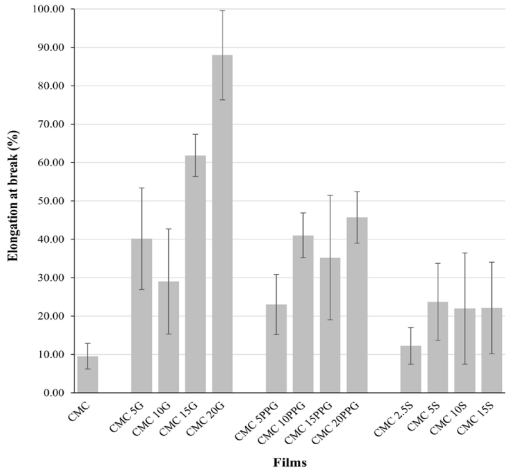

Figure 9: Elongation at break (%) of CMC films with varying plasticizer types and concentrations

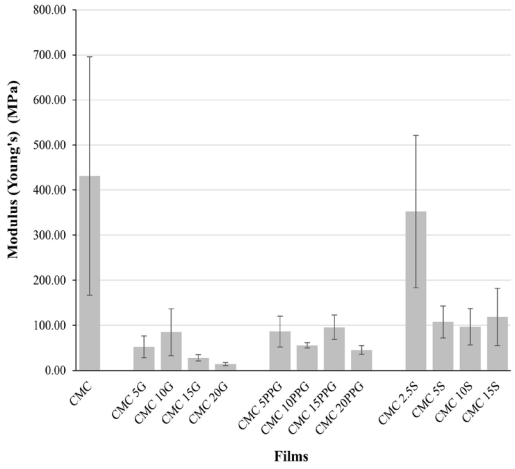

Figure 10: Young's modulus of CMC films in relation to plasticizer content and type

The tensile strength values obtained in this study are comparable to those reported by Anantachaisilp *et al*.,[30] who developed CMC films from water hyacinth cellulose using 25% PPG as a plasticizer. Their study reported a tensile strength of 14 MPa. In comparison, the present study found that CMC films plasticized with 20% PPG

exhibited a tensile strength of approximately 20 MPa, demonstrating similar performance trends.

The mechanical behavior of the plasticized CMC films can be attributed to the interaction between plasticizer molecules and the hydroxyl-rich CMC matrix. The incorporation of low-molecular-weight polyols disrupts intermolecular hydrogen bonding among CMC chains, leading to increased chain mobility and free volume. This effect is reflected in the progressive increase in elongation at break with increasing plasticizer content, accompanied by a reduction in tensile strength and Young's modulus. Among the plasticizers studied, G exhibited the most pronounced plasticizing efficiency, which can be explained by its smaller molecular size and higher density of hydroxyl groups, enabling stronger interactions with CMC chains compared to PPG and S.

Effect of plasticizer on thermal properties of CMC films

The thermal stability of CMC films derived from water hyacinth was evaluated using TGA under a nitrogen atmosphere. Four samples were compared: neat CMC film, CMC film with 20% G, CMC film with 20% PPG, and CMC film with 15% S. The TGA and derivative thermogravimetric (DTG) curves are presented in Figures 11 and 12, respectively. The relevant decomposition data are summarized in Table 2.

The TGA thermogram of the neat CMC film exhibited a typical three-stage degradation pattern. Initial weight loss occurred at 50.7 °C. This stage corresponds to the evaporation of bound water, with a minor mass loss of 3.5%. The main degradation stage was recorded around 260–310 °C. A major weight loss occurred due to the thermal decomposition of the CMC backbone, including depolymerization and degradation of the carboxymethyl substituents. The DTG peak was observed at 285.1 °C, indicating the temperature of maximum decomposition rate. A slow mass loss in final stage at 568.1 °C is associated with final breakdown and char oxidation. The film exhibited a residual weight of 13.5% at 600 °C, reflecting its carbonaceous char content.

CMC film plasticized with 20% G showed slightly lower thermal stability. The initial mass loss was slightly higher (6.0%) at 53.9 °C, which corresponds to the evaporation of water. The Td onset at second weight loss is around 250.0 °C, while the maximum of degradation occurs at 280.0 °C (DTG curve), which corresponds to the degradation of the cellulose backbone and carboxymethyl groups. The main degradation occurred at a lower temperature than the neat CMC film, indicating reduced thermal stability. The residual mass at 600 °C was lower than that of the neat film, suggesting that G decreases the thermal resistance of CMC due to its plasticizing effect, increasing chain mobility and facilitating earlier decomposition.

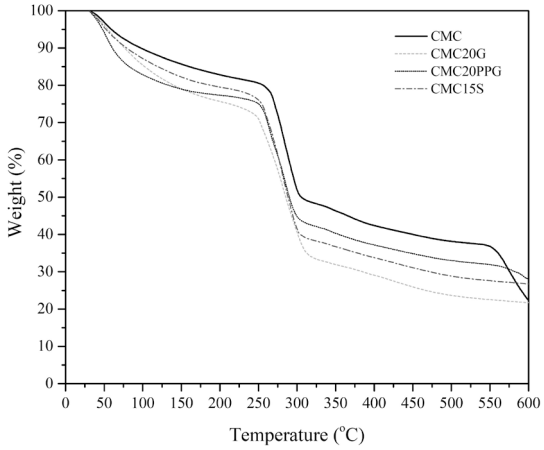

Figure 11: TGA thermograms of CMC films derived from water hyacinth: neat CMC film, CMC film with 20% glycerol (CMC 20G), CMC film with 20% propylene glycol (CMC 20PPG), and CMC film with 15% sorbitol (CMC 15S)

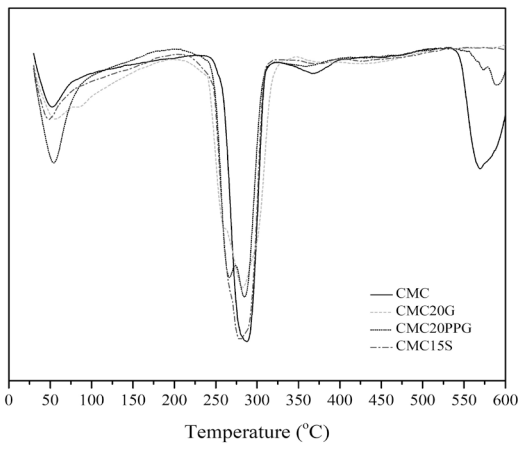

Figure 12: DTG thermograms of CMC films derived from water hyacinth: neat CMC film, CMC film with 20% glycerol (CMC 20G), CMC film with 20% propylene glycol (CMC 20PPG), and CMC film with 15% sorbitol (CMC 15S)

Table 2
Decomposition temperature (T_d) and %weight loss for CMC film and CMC films plasticized with varying plasticizer

Sample	T_d (°C)				%Weight loss		Residue at 600 °C (%)
	1st	2nd (onset)	2nd (peak)	3rd	1st	2nd	
CMC	50.7	260.0	285.1	568.1	3.5	48.5	13.5
CMC 20G	53.9	250.0	280.0	-	6.0	40.5	12.5
CMC 20PPG	52.8	263.9	284.0	-	9.0	39.0	10.0
CMC 15S	47.5	258.4	278.7	-	5.0	45.0	8.5

The TGA thermogram of the CMC film plasticized with 20% PPG shows two decomposition stages similar to the CMC 20G film. At 52.8 °C, the first step of water breakdown occurs, resulting in a weight loss of roughly 9.0%. The Td onset at the second stage was 263.9 °C and was attributed to the decomposition of the CMC backbone. A DTG peak with maximum degradation occurring at 284.0 °C. The decomposition profile suggests moderate thermal stability among the plasticized films. PPG, having a higher boiling point and lower hygroscopicity than G, contributes to a slightly higher onset degradation temperature. The residual mass of around 10% at 600 °C indicated more complete degradation.

The CMC film plasticized with 15% S exhibited lower initial weight loss due to adsorbed water than G- and PPG-plasticized films, starting near 47.5 °C. The Td onset at second step is 258.4 °C and Td peak is 278.7 °C. Both values are slightly lower than those of neat CMC, indicating a reduction in thermal stability.

All CMC films, both neat and plasticized, show an initial weight loss stage occurring at relatively low temperatures, typically around 47-54 °C. This stage is attributed to the evaporation of absorbed moisture and other volatile components. The percentage of weight loss in this stage varies from 3.5% (neat CMC), 5.0% (CMC 15S), 6.0% (CMC 20G) to 9.0% (CMC 20PPG). For plasticized films, especially CMC 20PPG, the slightly higher initial weight loss percentage might be attributed to the plasticizers increasing the hygroscopicity of the films, leading to more absorbed moisture.

The residue at 600 °C for plasticized films is lower than that for neat CMC: CMC 20G (12.5%), CMC 20PPG (10.0%), and CMC 15S (8.5%) compared to CMC (13.5%). This lower residue suggests that the plasticizers might promote a more complete degradation of the CMC polymer or themselves degrade more fully, leading to less char formation at higher temperatures.

Thermal analysis further supports the plasticization mechanism, as evidenced by the moderate decrease in degradation onset temperatures following plasticizer addition. The addition of plasticizers (G, PPG, and S) tends to slightly decrease the main decomposition temperature (the second stage) of the CMC film. This suggests that the plasticizers may reduce the intermolecular forces within the CMC matrix, making it easier for the polymer chains to degrade at lower temperatures. This is a common effect of plasticizers, as they increase the free volume and chain mobility.

Importantly, the observed thermal behavior remains within a range suitable for low temperature processing and disposable or short life applications. Overall, the results indicate that plasticizer selection provides an effective strategy to tailor the structure property relationships of invasive biomass derived CMC films, expanding their potential for sustainable polymer and packaging-related applications.

CONCLUSION

This work demonstrates the effective conversion of water hyacinth into CMC and its subsequent processing into homogeneous cellulose based films. Structural analyses confirmed successful carboxymethylation, accompanied by a reduction in crystallinity and the formation of an amorphous CMC matrix favorable for film formation. While neat CMC films exhibited relatively high stiffness and limited ductility, the incorporation of polyol plasticizers provided a systematic means to modify film performance. Increasing plasticizer content enhanced chain mobility, resulting in a pronounced increase in elongation at break and a concurrent decrease in tensile strength and Young's modulus. Among the plasticizers investigated, glycerol exhibited the

highest plasticization efficiency, whereas sorbitol showed limitations at higher loadings due to phase separation. Thermal analysis indicated a moderate reduction in degradation onset temperatures, consistent with increased polymer chain flexibility induced by plasticization. Overall, the study highlights the tunability of structure–property relationships in CMC films derived from the lignocellulosic biomass of an invasive species, contributing to the development of functional cellulose based materials through controlled chemical modification and formulation strategies.

ACKNOWLEDGMENTS: This work was funded by Thailand Science Research and Innovation (TSRI) and Maejo University's Office of Agricultural Research and Extension (project numbers MJU.1-67-10-004 and MJU.1-68-10-001 for fiscal years 2024 and 2025, respectively).

REFERENCES

[1] A. Malik, *Environ. Int.*, **33**, 122 (2007), https://doi.org/10.1016/j.envint.2006.08.004
[2] V. Guna, M. Ilangovan, M. G. A. Prasad and N. Reddy, *ACS Sustain. Chem. Eng.*, **5**, 4478 (2017), https://doi.org/10.1021/acssuschemeng.7b00051
[3] J. Yan, Z. Wei, Q. Wang, M. He, S. Li *et al.*, *Bioresour. Technol.*, **193**, 103 (2015), https://doi.org/10.1016/j.biortech.2015.06.069
[4] A. F. Abdel-Fattah and M. A. Abdel-Naby, *Carbohyd. Polym.*, **87**, 2109 (2012), https://doi.org/10.1016/j.carbpol.2011.10.033
[5] S. M. Gaonkar and P. R. Kulkarni, *Acta Polym.*, **37**, 189 (1986), https://doi.org/10.1002/actp.1986.010370317
[6] H. Suryadi, Sutriyo, H. R. Sari and D. Rosikhoh, *J. Young Pharm.*, **9**, s19 (2017), https://doi.org/10.5530/jyp.2017.1s.6
[7] F. Fitrya, N. A. Fithri, D. P. Wijaya and E. P. Sembiring, *Trop. J. Nat. Prod. Res.*, **5**, 503 (2021), http://repository.unsri.ac.id/id/eprint/48067
[8] T. Semachai, P. Chandranupap and P. Chandranupap, *MATEC Web Conf.*, **187**, 02003 (2018), https://doi.org/10.1051/matecconf/201818702003
[9] R. Sothornvit and J. M. Krochta, "Food Science and Technology", Academic Press, 2005, pp. 403, https://doi.org/10.1016/B978-012311632-1/50055-3
[10] S. A. Asl, M. Mousavi and M. Labbafi, *J. Food Process. Technol.*, **8**, 1000687 (2017), https://doi.org/10.4172/2157-7110.1000687
[11] S. A. Laith and A. G. Al-Hashimi, *Basrah J. Agric. Sci.*, **32**, 68 (2019), https://doi.org/10.37077/25200860.2019.129
[12] T. Tianmee, U. Ratanakamnuan and P. Namwong, *J. Phys. Conf. Ser.*, **2888**, 012010 (2024), https://doi.org/10.1088/1742-6596/2888/1/012010
[13] S. D. Pasini Cabello, E. A. Takara, J. Marchese and N. A. Ochoa, *Mater. Chem. Phys.*, **162**, 491 (2015), https://doi.org/10.1016/j.matchemphys.2015.06.019
[14] M. L. Sanyang, S. M. Sapuan, M. Jawaid, M. R. Ishak and J. Sahari, *J. Food Sci. Technol.*, **53**, 326 (2016), https://doi.org/10.1007/s13197-015-2009-7
[15] A. Phumkacha, T. Leejarkpai and S. Kirdponpattara, *Mater. Sci. Forum*, **1098**, 65 (2023), https://doi.org/10.4028/p-NBII0n
[16] S. Bhatia, A. Al-Harrasi, I. H. Almohana, M. F. Albayati, M. Jawad *et al.*, *Heliyon*, **10**, e24210 (2024), https://doi.org/10.1016/j.heliyon.2024.e24210
[17] S. Paude, S. Regmi and S. Janaswamy, *Food Packag. Shelf Life*, **37**, 101090 (2023), https://doi.org/10.1016/j.fpsl.2023.101090
[18] P. Rachtanapun, S. Luangkamin, K. Tanprasert and R. Suriyatem, *LWT - Food Sci. Technol.*, **48**, 52 (2012), https://doi.org/10.1016/j.lwt.2012.02.029
[19] S. Kamthai and R. Magaraphan, *Ind. Crop. Prod.*, **109**, 753 (2017), https://doi.org/10.1016/j.indcrop.2017.09.040
[20] B. K. Barai, R. S. Singhal and P. R. Kulkarni, *Carbohyd. Polym.*, **32**, 229 (1997), https://doi.org/10.1016/S0144-8617(96)00166-X
[21] M. L. R. Simone, R. Noor, I. G. de M. Maria, S. M. B. N. Sônia and C. I. D. B. Clara, *Carbohyd. Polym.*, **87**, 1131 (2012), https://doi.org/10.1016/j.carbpol.2011.08.084
[22] M. K. Mohamad Haafiz, S. J. Eichhorn, A. Hassan and M. Jawaid, *Carbohyd. Polym.*, **93**, 628 (2013), https://doi.org/10.1016/j.carbpol.2013.01.035
[23] N. Johara, I. Ahmad and A. Dufresne, *Ind. Crop. Prod.*, **37**, 93 (2012), https://doi.org/10.1016/j.indcrop.2011.12.016
[24] M. T. Baker and O. S. Oguntoye, *J. Turk. Chem. Soc. A*, **10**, 31 (2023), https://doi.org/10.18596/jotcsa.1107627
[25] J.-F. Su, Z. Huang, X.-Y. Yuan, X.-Y. Wang and M. Li, *Carbohyd. Polym.*, **79**, 145 (2010), https://doi.org/10.1016/j.carbpol.2009.07.035
[26] S. Gupta and P. K. Varshney, *Polym. Bull.*, **76**, 6169 (2019), https://doi.org/10.1007/s00289-019-02714-1
[27] H. Suryanto, D. Syukri, A. Faridah, U. Yanuhar, J. Selvi Binoj *et al.*, *MESI*, **5**, 5 (2025), https://doi.org/10.31603/mesi.12789
[28] P. Basu, U. Narendrakumar, R. Arunachalam, S. Devi and I. Manjubala, *ACS Omega*, **3**, 12622 (2018), https://doi.org/10.1021/acsomega.8b02015
[29] T. Tamara, Sumari, Nazriati and S. Arni, *IOP Conf. Ser.: Earth Environ. Sci.*, **456**, 012077 (2020), https://doi.org/10.1088/1755-1315/456/1/012077
[30] S. Anantachaisilp, S. Siripromsombut, T. Ruansoong and T. Kwamman, *J. Phys. Conf. Ser.*, **1719**, 012110 (2020), https://doi.org/10.1088/1742-6596/1719/1/012110